



NONLINEAR FLUID FORCES IN CYLINDRICAL SQUEEZE FILMS. PART I: SHORT AND LONG LENGTHS

Y. HAN

AECL, Chalk River, Ontario, Canada K0J 1J0

AND

R. J. ROGERS

*Department of Mechanical Engineering, University of New Brunswick
Fredericton, NB, Canada E3B 5A3*

(Received 13 June 1999, and in final form 27 June 2000)

Using three approximation methods, nonlinear models have been derived for short and long cylindrical squeeze films with arbitrary inner cylinder motions. Elliptical and parabolic velocity profiles are employed in the derivation in order to determine the effects of the choice of velocity profile. The only differences in the final squeeze film equations, due to the three approximation methods and the two velocity profiles, are in the four constant coefficients. Each term in the squeeze film equations is a nonlinear function of cylinder position. Comparing the present nonlinear expressions with existing models for short cylindrical squeeze films shows that the force terms are either exactly the same or have the same trends with instantaneous eccentricity values. For long cylindrical squeeze films, the present expressions have some force terms which are essentially the same as in other studies, while other force terms show variations with position which are very different from a previously published study. © 2001 Academic Press

1. INTRODUCTION

CYLINDRICAL SQUEEZE FILMS are important to design and maintenance engineers working with squeeze film dampers in rotating machinery, as well as other industrial applications such as shell-and-tube heat exchangers, because of the increasing demand for mechanical systems (for example, in the nuclear power industry) to have long life and satisfactory operating performance. The study of squeeze films, generated in a fluid-filled clearance between a cylinder (tube) and a cylindrical sleeve (support) when the cylinder oscillates, is important for the prediction of the cylinder motions, contact forces and the rate of fretting wear (Pettigrew & Ko 1980). The damping provided by the squeeze films is the major source of damping to limit the vibration induced by turbulent liquid flow across the heat exchanger tubes (Pettigrew *et al.* 1986).

To evaluate and improve the performance of the shell-and-tube heat exchangers, many theoretical and experimental investigations on the squeeze film phenomena acting between a tube and its support have been initiated in the past. The main contributors to this work are Mulcahy (1980), Haslinger *et al.* (1990), Esmonde *et al.* (1992) and Lu & Rogers (1992, 1994, 1995).

Because of the common theoretical basis, the study of squeeze films between tubes and support plates in heat exchangers is closely related to that of squeeze film dampers used in rotating machinery. However, due to the differences in the structures and movement

characteristics of the inner cylinder, most of the analyses in the literature of squeeze film studies in heat exchangers consider finite length film approximations and special considerations are given to arbitrary inner cylinder motion. Two of the analytical approaches available in the literature for modelling finite-length squeeze films are: (i) to use length-correction factors with a short axial flow solution, and (ii) to use side-leakage factors with an infinitely long circumferential flow solution. A relevant example of modelling finite-length squeeze films by using length-correction factors with a short film solution is given by Barrett *et al.* (1980). Modelling finite-length squeeze films by using side-leakage factors with an infinitely long circumferential solution, can be seen, for example, from the publications by Warner (1963), San Andres & Vance (1987*a*) and Lu & Rogers (1994). Zhang & Roberts (1996) also used the same or similar ideas to account for the length effects. The validity of this way of forming the force equations is naturally dependent on the accuracy of the short and long squeeze film models.

There are many publications of theoretical and experimental studies on squeeze film dampers dealing with short and long bearing models. For short models, Tichy (1982) presented an approximate analytical solution for squeeze film damper forces, which accounts for the effects of fluid inertia and viscoelasticity. An earlier "exact" solution for infinitesimal oscillation amplitudes is extended to finite amplitudes using the Rivlin-Ericksen second-order fluid. In a later paper, Tichy (1985) experimentally studied short squeeze-film bearing forces including inertia effects for squeeze Reynolds number ($\omega c^2/\nu$) up to 13 and eccentricity ratios up to 0.8. The ratio of length/diameter was close to 0.15. San Andres *et al.* (1993) carried out an experimental study on squeeze film forces for a short squeeze film damper with length/diameter ratio of 0.188. Zhang *et al.* (1993, 1994) and Zhang (1997) also performed theoretical and experimental studies of short squeeze film dampers. The results of the above studies were for applications with small to moderate squeeze Reynolds number cases.

The significant studies of squeeze film damper performance for long bearing cases are: (i) small-amplitude circular-centred motions by Tichy (1984), San Andres & Vance (1987*a, b*) and Jung (1990); (ii) periodic motions by Zhang (1997); and (iii) arbitrary motions by El-Shafei & Crandall (1991). They all tried to include fluid inertia effects in the infinitely long squeeze films. In the first and the second categories only the transient inertia term was considered (with the statement that convective inertia terms were all negligible relative to the transient term). One of the very fundamental assumptions in the El-Shafei & Crandall study is that the effects of the fluid inertia on the velocity profile can be neglected. Therefore, the applications of their studies are also limited to the fluids with small to moderate Reynolds number.

There are relatively few publications on the study of squeeze films between tubes and support plates in heat exchangers. Lu & Rogers (1992) developed an equation for the short length, cylindrical squeeze film forces with moderately large eccentricities based on a squeeze film model for two-dimensional rectangular plates. Lu & Rogers (1994) developed an infinitely long cylindrical model with radial inner cylinder motions by using an averaging procedure (across the film thickness) to include all inertia terms. Due to the large radial clearance (typically $R/c = 30-50$) and the low viscosity fluid used, the squeeze Reynolds number in shell-and-tube heat exchangers is usually higher than that in squeeze film dampers. Consequently, this difference in squeeze Reynolds numbers requires attention for squeeze film studies in heat exchanger applications. Until now there is no theoretical study dealing with infinitely long squeeze films between a tube and a heat exchanger support plate for arbitrary tube motions.

The objective of the present work is to develop both a short squeeze film model and an infinitely long model suitable for accurate prediction of the squeeze film forces between

tubes and their supports in heat exchangers, with consideration of the various kinds of inertia effects. The derivation of the short model is similar to that of Lu & Rogers (1995), whereas for the long model, a new elliptical velocity distribution has been derived. The results obtained using the different velocity profiles and three approximation methods are compared with the existing models. The present paper is an expanded version of a conference paper (Han & Rogers 1997).

2. SHORT CYLINDRICAL MODEL

2.1. DERIVATION

Figure 1 shows the cylindrical squeeze film configuration for the short model and the coordinates used. The cylinder centre O' has an instantaneous position (e, ψ) in the stationary polar coordinate system, and n and t are moving unit vectors. The film thickness at any angle θ in polar coordinates is

$$h = c - e \cos(\phi - \psi) = c - e \cos \theta, \quad (1)$$

see Nomenclature in Appendix B for variable definitions.

If we neglect the effect of the convective inertia of fluid entering and exiting the system, the squeeze film pressure for the short cylindrical model is given by an expression derived for rectangular plates (Han & Rogers 1996)

$$p - p_a = \left(D_1 \frac{\mu}{h^3} \frac{dh}{dt} + D_2 \frac{\rho}{h} \frac{d^2h}{dt^2} - D_3 \frac{\rho}{h^2} \left(\frac{dh}{dt} \right)^2 \right) \left(\frac{X^2}{2} - \frac{L^2}{8} \right). \quad (2)$$

The constant D_i coefficients depend on the choice of approximation method, the type of flow velocity profile, and also the profile factor A for the elliptical velocity profile as shown in Tables 1 and 2. Differentiating the local clearance h twice with respect to time and

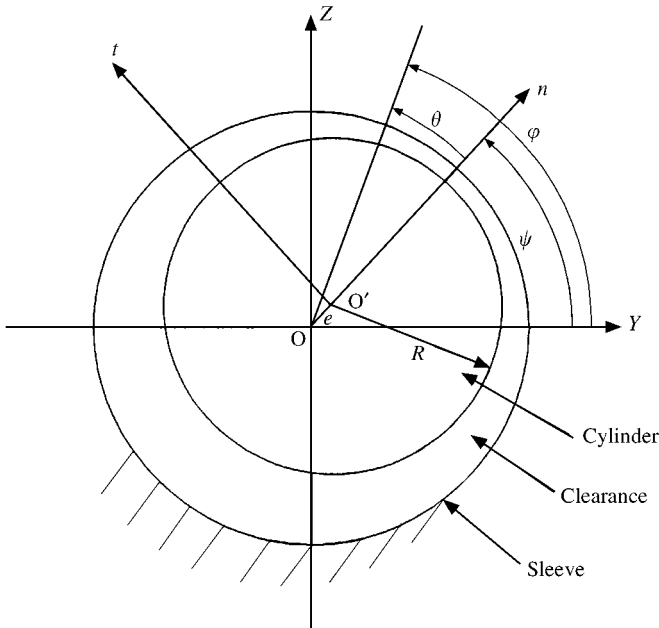


Figure 1. Configuration of squeeze film for short cylindrical model with arbitrary cylinder motion.

TABLE 1
Constant coefficients for parabolic velocity profiles*

Profile	Method	D_1	D_2	D_3	D_4
Parabolic	Momentum	12	1	2.4	1.2
	Iterative	12	1	2.914	1.543
	Energy	12	1	2.914	1.543

* The results of momentum and energy approximations using parabolic velocity profile are from El-Shafei and Crandall (1991).

TABLE 2
Constant coefficients for elliptical profiles and different A values

Method	A value	D_1	D_2	D_3	D_4
Momentum approx.	1	∞	1	2.162	1.081
	1.1	18.925	1	2.293	1.147
	1.2	15.998	1	2.324	1.162
Iterative approx.	1	12	1.125	2.479	1.297
	1.1	12	1.17	2.719	1.435
	1.2	12	1.18	2.775	1.466
Energy approx.	1	∞	1.081	2.364	1.216
	1.1	12.682	1.147	2.657	1.389
	1.2	12.308	1.162	2.731	1.432

substituting the results into the above equation yields the film pressure as a function of the axial coordinate X and θ ,

$$p = p_c \left(\frac{4X^2}{L^2} - 1 \right) + p_a, \tag{3}$$

where

$$\begin{aligned}
 p_c \frac{8}{L^2} = & -\frac{D_1 \mu \cos \theta}{c^3(1 - \varepsilon \cos \theta)^3} \dot{e} - \frac{D_1 \mu \sin \theta}{c^3(1 - \varepsilon \cos \theta)^3} e \dot{\psi} - \frac{D_2 \rho \cos \theta}{c(1 - \varepsilon \cos \theta)} \ddot{e} - \frac{D_2 \rho \sin \theta}{c(1 - \varepsilon \cos \theta)} e \ddot{\psi} \\
 & - \frac{D_2 \rho \sin \theta}{c(1 - \varepsilon \cos \theta)} 2\dot{e} \dot{\psi} + \frac{D_2 \rho \cos \theta}{c(1 - \varepsilon \cos \theta)} e \dot{\psi}^2 - \frac{D_3 \rho \cos^2 \theta}{c^2(1 - \varepsilon \cos \theta)^2} \dot{e}^2 \\
 & - \frac{D_3 \rho \sin^2 \theta}{c^2(1 - \varepsilon \cos \theta)^2} (e \dot{\psi})^2 - \frac{D_3 \rho \cos \theta \sin \theta}{c^2(1 - \varepsilon \cos \theta)^2} 2e \dot{e} \dot{\psi}.
 \end{aligned}$$

Taking p_a as atmospheric pressure, we can obtain the squeeze film force acting on a very small arc of the cylinder with width $R d\theta$:

$$dF = \left(\int_{-L/2}^{L/2} p_c \left(\frac{4X^2}{L^2} - 1 \right) dX \right) R d\theta = -\frac{2Lp_c R}{3} d\theta. \tag{4}$$

In the conventional way, the forces acting on the moving cylinder in the normal and tangential directions can be obtained as

$$F_n = -C_1 C_v^n \dot{e} - C_2 M_{un}^n \ddot{e} - C_2 M_{cv} \frac{\dot{e}^2}{e} + C_2 M_{ce} e \dot{\psi}^2, \tag{5}$$

$$F_t = -C_1 C_v^t e \dot{\psi} - C_2 M_{un}^t e \ddot{\psi} - C_2 M_{co} 2\dot{e} \dot{\psi}. \tag{6}$$

TABLE 3
Geometry and force coefficients of the short cylindrical model

C_1	$\frac{\mu L^3 R}{c^3}$	C_2	$\frac{\rho L^3 R}{c}$
C_v^n	$\frac{D_1}{12} I_3^{02}$	C_v^t	$\frac{D_1}{12} I_3^{20}$
M_{un}^n	$\frac{D_2}{12} I_1^{02}$	M_{un}^t	$\frac{D_2}{12} I_1^{20}$
M_{cv}	$\frac{\varepsilon D_3}{12} I_2^{03}$	M_{co}	$\frac{D_2}{12} I_1^{20} + \frac{\varepsilon D_3}{12} I_2^{21}$
M_{ce}	$\frac{D_2}{12} I_1^{02} - \frac{\varepsilon D_3}{12} I_2^{21}$		

TABLE 4
Force coefficients of the short cylindrical model for 2π films

C_v^n	$\frac{D_1 \pi}{12} \frac{1 + 2\varepsilon^2}{\gamma^5}$	C_v^t	$\frac{D_1}{12} \frac{\pi}{\gamma^3}$
M_{un}^n	$\frac{D_2 \pi}{6} \frac{1 - \gamma}{\varepsilon^2 \gamma}$	M_{un}^t	$\frac{D_2}{6} \frac{\pi(1 - \gamma)}{\varepsilon^2}$
M_{cv}	$\frac{D_3 \pi}{6\varepsilon^2} \left(2 - \frac{2 - 3\varepsilon^2}{\gamma^3} \right)$	M_{co}	$\frac{\pi(1 - \gamma)}{6\varepsilon^2} \left(D_2 + \frac{D_3(1 - \gamma)}{\gamma} \right)$
M_{ce}	$\frac{\pi(1 - \gamma)}{6\varepsilon^2 \gamma} [D_2 - D_3(1 - \gamma)]$		

The normal squeeze film force expressed by equation (5) consists of four terms. The first three terms are the viscous term, unsteady inertia term and convective inertia term, respectively, and the fourth term is the centripetal inertia term induced by the centripetal acceleration of the cylinder centre. The tangential squeeze film force expressed by equation (6) consists of three terms. The first two terms are the viscous and the unsteady inertia terms, while the third term is the Coriolis inertia term, induced by the Coriolis acceleration of the cylinder centre. The geometry coefficients and the force coefficients in the above equations are listed in Table 3, where the integral terms are defined as (Booker 1965)

$$I_n^{lm} = \int_{\theta_1}^{\theta_2} \frac{\sin^l \theta \cos^m \theta}{(1 - \varepsilon \cos \theta)^n} d\theta.$$

For applications in heat exchangers with water as the fluid, the integral limit of $(0, 2\pi)$ should be used in the above equations, since usually there is no cavitation and therefore a full film is formed in the system. The force coefficients for the 2π -film after integration are listed in Table 4.

2.2. DISCUSSION

To calculate the squeeze film forces, three approximation methods have been used by Han (1997) and Han & Rogers (1996). All three methods require an approximation for the

velocity profile in the squeeze flow. Comparing equations (5) and (6) with the force equations from Lu (1993) and El-Shafei & Crandall (1991) for the short model, we can see that the only differences are caused by the constant coefficients D_i ($i = 1, 2$ and 3) (Han & Rogers 1996), when the pressure difference induced by the edge effect in Lu's study is neglected. Substituting the values of the constant coefficients obtained by Han & Rogers (1996) for the energy method with the conventional parabolic velocity profile into equations (5) and (6), we will reproduce exactly the same results as in the El-Shafei & Crandall paper. Performing the same substitution for the momentum method, we will find that the differences in the results from Lu's study are only due to the edge effect.

Zhang *et al.* (1993) also developed analytical expressions for a short cylindrical squeeze film damper and used both the momentum and energy approximation methods. By comparing the pressure expressions (see Table 1 in Zhang *et al.*, 1993) with the studies from Tichy and Bou-Said (1991), El-Shafei and Crandall (1991), their own study and others, the differences in the temporal inertia term and convective inertia term are shown to be due to the different averaging methods used within the squeeze film thickness.

Similar to what Zhang *et al.* found, the differences between the present study and other studies are only in the constant coefficients and the differences are generally not large (Han 1997). The ratio of unsteady inertia force terms obtained using the elliptical profile and the parabolic velocity profile derived by El-Shafei and others ranges from 1.081 to 1.180 for shape factor $A = 1.0$ – 1.2 when the iterative or energy approximation methods are utilized. The ratios greater than unity show that the elliptical velocity profile takes more inertia effect into account than does the parabolic velocity profile. The experimental results by Lu & Rogers (1992, 1994), El-Shafei (1988) and San Andes *et al.* (1993) demonstrated that when the cylinder (journal) motion amplitude increases, the unsteady inertia term increases and dominates over the other force terms. Thus, if we have accurate unsteady inertia terms, we will have more accurate squeeze film force equations for a system with large amplitude motion.

3. LONG CYLINDRICAL MODEL

3.1. DERIVATION

Figure 2 shows the cylindrical squeeze film configuration and coordinates used for the long model configuration. The x , y and z (normal to the page) coordinates constitute the local coordinate system for the squeeze film at an angle θ , where u is the local fluid flow velocity at this angle along the x direction. The other notations are the same as for the short model. The simplified Navier–Stokes equation for the infinitely long cylindrical squeeze film can be written as

$$\rho \left(\frac{\partial u}{\partial t} + u \frac{\partial u}{R \partial \theta} + v \frac{\partial u}{\partial y} \right) = - \frac{\partial p}{R \partial \theta} + \mu \frac{\partial^2 u}{\partial y^2}, \quad (7)$$

where $\partial p / \partial y = 0$ since the variation of pressure across the film is small and can be neglected and $\partial p / \partial z = 0$ since L is infinite (z is normal to page). The continuity equation is

$$\frac{\partial u}{R \partial \theta} + \frac{\partial v}{\partial y} = 0. \quad (8)$$

To solve these equations, the same strategy as in Han & Rogers (1996) is used. The elliptical velocity distributions obtained for the rectangular model can be further developed to form the distributions for the long cylinder model.

After obtaining Q , the mean out-flow velocity at angle θ is easy to determine using

$$\bar{u} = \frac{Q}{h} = \frac{R}{h} v'_c, \tag{14}$$

where v'_c is the integral of $-v_c$ with respect to θ from 0 to θ ,

$$v'_c = \dot{e} \sin \theta - e \dot{\psi} \cos \theta + e \dot{\psi}. \tag{15}$$

Because the flow is described using an elliptical profile, we can also have the expression for the mean out-flow velocity given as

$$\bar{u} = \int_0^h C(E_1 - E_2) dy. \tag{16}$$

Through making the integral and re-arranging equation (16) for C , we obtain

$$C = \frac{2R}{Bh^2} v'_c. \tag{17}$$

Therefore, the final form of the circumferential flow velocity is given by

$$u = \frac{2R}{Bh} (E_1 - E_2) v'_c. \tag{18}$$

From the continuity equation (8) and taking into account that $\phi - \psi = \theta$, so $\dot{\psi} = -\dot{\theta}$, $\partial \dot{\psi} / \partial \theta = 0$, and $\partial h / \partial \theta = e \sin \theta$, we find

$$\begin{aligned} v &= - \int \frac{\partial u}{R \partial \theta} dy \\ &= \frac{2}{Bh^2} \left[\left(\frac{1}{4} ((2y - h)E_1 h + (Ah)^2 E_3) - hyE_2 \right) v_c + (E_1 - E_2) y v'_c e \sin \theta \right] + C', \end{aligned} \tag{19}$$

where

$$\frac{\partial u}{R \partial \theta} = - \frac{2}{Bh} (E_1 - E_2) v_c + \frac{2}{Bh^2} \left(\frac{A^2 h + (2y - h)}{E_1 h} - 2E_1 + E_2 \right) v'_c e \sin \theta.$$

The constant C' can be determined through utilizing the boundary condition $y = 0, v = 0$,

$$C' = \frac{1}{2B} (A^2 E_4 + E_2) v_c. \tag{20}$$

Substituting equation (20) into equation (19), we have the expression for the velocity distribution in the y direction

$$v = \frac{1}{2Bh} [(2y - h)E_1 + A^2 h(E_3 + E_4) + E_2(h - 4y)] v_c + \frac{2}{Bh^2} (E_1 - E_2) y v'_c e \sin \theta. \tag{21}$$

Through the same procedure as above, we can obtain the velocity distributions for the long cylindrical model based on the parabolic velocity profile as

$$u = \frac{6R}{h^3} (hy - y^2) v'_c, \tag{22}$$

$$v = \frac{6}{h^4} \left[\left(\frac{h^2 y^2}{2} - \frac{hy^3}{3} \right) v_c + (hy^2 - y^3) v'_c e \sin \theta \right]. \tag{23}$$

El-Shafei (1988) also derived the velocity distributions using Reynolds' equation for a long model. The difference between the velocity distributions expressed by equations (22) and (23) and those obtained by El-Shafei is in the third term of expression v'_c , that is $3\epsilon/(2 + \epsilon^2)$. [El-Shafei's equivalent to expression (15) is $v'_c = \dot{\epsilon} \sin \theta - e\dot{\psi} \cos \theta + e\dot{\psi}3\epsilon/(2 + \epsilon^2)$ which is not based on the integral of $-v_c$.]

Based on Navier–Stokes equation (7) and using the three approximation methods, as well as the elliptical and the present parabolic velocity distributions (18) and (21)–(23), the general pressure gradients are derived in Appendix A and can be expressed as

$$\frac{\partial p}{\partial \theta} = \frac{\mu R^2}{h^3} D_1 v'_c - \frac{\rho R^2}{h} D_2 C_t^1 - \frac{\rho R^2}{h^2} D_3 C_t^2 + \frac{\rho R^2}{h^3} D_4 C_\theta^2, \quad (24)$$

where C_t^1 , C_t^2 and C_θ^2 are defined in Appendix A and D_i ($i = 1-4$) are the constant coefficients listed in Tables 1 and 2.

The squeeze film forces acting on the surface of the moving cylinder can be expressed by the following equations:

$$\begin{aligned} F_n &= -RL \int_{\theta_1}^{\theta_2} p \cos \theta \, d\theta \\ &= -RL[p \sin \theta]_{\theta_1}^{\theta_2} + RL \int_{\theta_1}^{\theta_2} \frac{\partial p}{\partial \theta} \sin \theta \, d\theta, \end{aligned} \quad (25)$$

$$\begin{aligned} F_t &= -RL \int_{\theta_1}^{\theta_2} p \sin \theta \, d\theta \\ &= RL[p \cos \theta]_{\theta_1}^{\theta_2} - RL \int_{\theta_1}^{\theta_2} \frac{\partial p}{\partial \theta} \cos \theta \, d\theta. \end{aligned} \quad (26)$$

Integrating these equations by parts, the general squeeze film forces acting on the moving cylinder for a 2π film can be expressed as

$$F_n = -C_1 C_v^n \dot{\epsilon} - C_2 M_{un}^n \ddot{\epsilon} - C_2 M_{cv} \frac{\dot{\epsilon}^2}{e} + C_2 M_{ce} e \dot{\psi}^2, \quad (27)$$

$$F_t = -C_1 C_t^t e \dot{\psi} - C_2 M_{un}^t e \ddot{\psi} - C_2 M_{co} 2\dot{\epsilon} \dot{\psi}. \quad (28)$$

The same form of equations as for the short model are obtained. The geometry coefficients C_i ($i = 1-3$) and force coefficients C_v^n , M_{un}^n , M_{cv} , M_{ce} , C_t^t , M_{un}^t and M_{co} in the above equations are listed in Table 5.

3.2. DISCUSSION

Lu (1993) and El-Shafei & Crandall (1991) obtained the same form of equations for the infinitely long geometries for the applications of heat exchangers and squeeze film dampers, respectively, although Lu's study is for radial motion only. When the oscillation amplitude of the inner cylinder (or journal) increases or decreases for the same form of motion (radial or arbitrary motion), some of the force coefficients obtained here vary with very similar tendencies as their results, while others do not. Since all the force coefficients from Lu's study are very similar to the present work, as well as to El-Shafei & Crandall's studies, his results are not included in this paper.

For comparison, the force coefficients of the present approximation method in equations (27) and (28) and the corresponding force coefficients from El-Shafei & Crandall (1991) for the long model are listed in Table 6. In the present study, the differences due to the three approximation methods and the two profiles (elliptical and parabolic) are entirely

TABLE 5
Geometry and force coefficients for the long cylindrical model for 2π -films

C_1	$\frac{\mu R^3 L}{c^3}$	C_2	$\frac{\rho R^3 L}{c}$
C_v^n	$D_1 \frac{[F_{11}^n]_0^{2\pi}}{\dot{e}}$	C_3	$\frac{\rho R^3 L}{c^2}$
M_{un}^n	$D_2 \frac{[F_{21}^n]_0^{2\pi}}{\dot{e}}$	C_v^t	$-D_1 \frac{[F_{12}^t]_0^{2\pi}}{e\dot{\psi}}$
M_{cv}	$\frac{\varepsilon}{\dot{e}^2} \left(D_3 F_{31}^n - \frac{D_4}{c} F_{41}^n \right)_0^{2\pi}$	M_{un}^t	$-D_2 \frac{[F_{23}^t]_0^{2\pi}}{e\dot{\psi}}$
M_{ce}	$\frac{1}{e\dot{\psi}^2} \left(-D_2 F_{24}^n - \frac{D_3}{c} F_{33}^n + \frac{D_4}{c^2} F_{43}^n \right)_0^{2\pi}$	M_{co}	$\frac{1}{2e\dot{\psi}} \left(-D_2 F_{22}^t - \frac{D_3}{c} F_{32}^t + \frac{D_4}{c^2} F_{42}^t \right)_0^{2\pi}$

Note. The force components F_{ij} (i and j can be 1, 2, 3 or 4) are given in Han (1997).

TABLE 6
Force coefficients for the long cylindrical model for 2π film after integration

	Present	El-Shafei & Crandall
C_v^n	$D_1 \frac{\pi}{\gamma^3}$	$12 \frac{\pi}{\gamma^3}$
M_{un}^n	$D_2 \frac{2\pi}{\varepsilon^2} (1 - \gamma)$	$\frac{24\pi}{10\varepsilon^2} (1 - \gamma)$
M_{cv}	$-\frac{2\pi}{\varepsilon^2} \left[D_3 \left(2 - \frac{2 - \varepsilon^2}{\gamma} \right) + D_4 \left(\frac{6 - 3\varepsilon^2}{2\gamma} - 3 \right) \right]$	$-\frac{24\pi}{10\varepsilon^2} \left(1 - \frac{2 - \varepsilon^2}{2\gamma} \right)$
M_{ce}	$\frac{2\pi}{\varepsilon^2} \left[D_2 (1 - \gamma) - D_3 \left(2 - \varepsilon - \frac{(1 - \varepsilon)(2 + \varepsilon)}{\gamma} \right) \right]$ $-\frac{2\pi}{\varepsilon^2} \left[D_4 \left(2\varepsilon - 3 + \frac{(1 - \varepsilon)(8\varepsilon + \varepsilon^2 + 6)}{2\gamma(1 + \varepsilon)} \right) \right]$	$\frac{24\pi}{10(2 + \varepsilon^2)^2} \left(12 - \frac{2(10 - \varepsilon^2)\gamma}{2 + \varepsilon^2} \right)$
C_v^t	$\frac{3\pi D_1}{\gamma^5} (1 - \varepsilon)^2$	$\frac{24\pi}{(2 + \varepsilon^2)\gamma}$
M_{un}^t	$\frac{2\pi D_2}{\varepsilon^2 \gamma} [(1 - \gamma)(1 - 2\varepsilon) + \varepsilon^2]$ $\frac{\pi D_2}{\varepsilon^2 \gamma (1 + \varepsilon)} (2 - \varepsilon - 2\varepsilon^2 + \varepsilon^3 - 2\gamma + \varepsilon\gamma + 3\varepsilon^2\gamma)$	$\frac{24\pi}{10\varepsilon^2(2 + \varepsilon^2)} \left(\frac{4\gamma^3}{2 + \varepsilon^2} + 5\varepsilon^2 - 2 \right)$
M_{co}	$+\frac{\pi D_3}{\varepsilon^2 \gamma (1 + \varepsilon)} (-4 - \varepsilon + 5\varepsilon^2 + 4\gamma + \varepsilon\gamma - 3\varepsilon^2\gamma)$ $-\frac{\pi D_4}{\varepsilon^2 \gamma (1 + \varepsilon)} (-6 - 2\varepsilon + 7\varepsilon^2 + 6\gamma + 2\varepsilon\gamma - 4\varepsilon^2\gamma + \varepsilon^3)$	$\frac{24\pi}{10(2 + \varepsilon^2)^2} \left(12 - \frac{2(10 - \varepsilon^2)\gamma}{2 + \varepsilon^2} \right)$

contained in the four constant D_i coefficients listed in Tables 1 and 2. Except for the D_i constants, each individual term in the present force equations, from the different methods and profiles, is identical. Therefore, for convenience, the comparison carried out here is based on the present energy method and the present parabolic velocity profile.

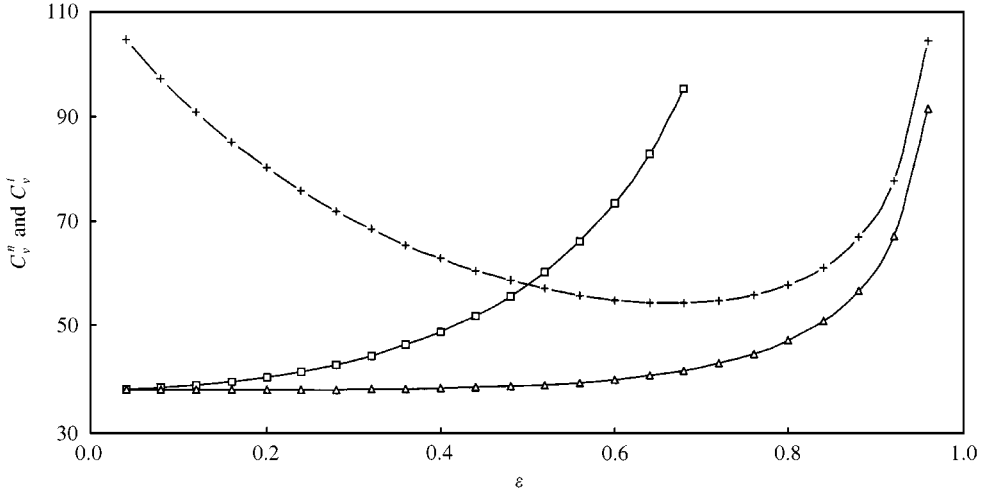


Figure 3. Viscous force coefficient comparison for long model: —□—, C_v^n (El-Shafei & Crandall and present); — + —, C_v^t (present); —△—, C_v^t (El-Shafei & Crandall).

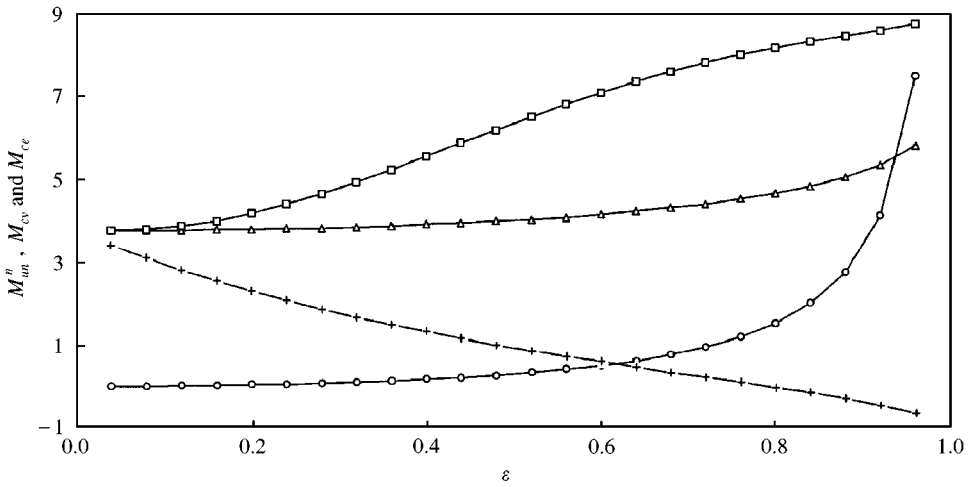


Figure 4. Normal inertia force coefficient comparison for long model: —□—, M_{ce} (El-Shafei & Crandall); —△—, M_{in}^n (El-Shafei & Crandall and present); — + —, M_{ce} (present); —○—, M_{cv} (El-Shafei & Crandall and present).

From Table 6, we can see that the present approximation methods and El-Shafei’s energy method for the squeeze film forces yield quite different equations. The differences are caused by (i) the velocity profile differences in the third term of v'_c , that is $3\epsilon/(2 + \epsilon^2)$, and (ii) the different derivation methods.

Figures 3–5 show comparisons of the viscous and inertia force coefficients in the normal and tangential directions between the present study and the El-Shafei & Crandall (1991) studies for a 2π -film. In the normal direction all the force coefficients except for centripetal inertia M_{ce} are exactly the same. When the instantaneous eccentricity ratio is close to zero ($\epsilon \rightarrow 0$), the differences between the M_{ce} values from the two studies decrease. At the other limit condition, when $\epsilon \rightarrow 1$, we can see very large differences in the M_{ce} inertia force coefficient. Greater differences between the two studies are shown in the tangential

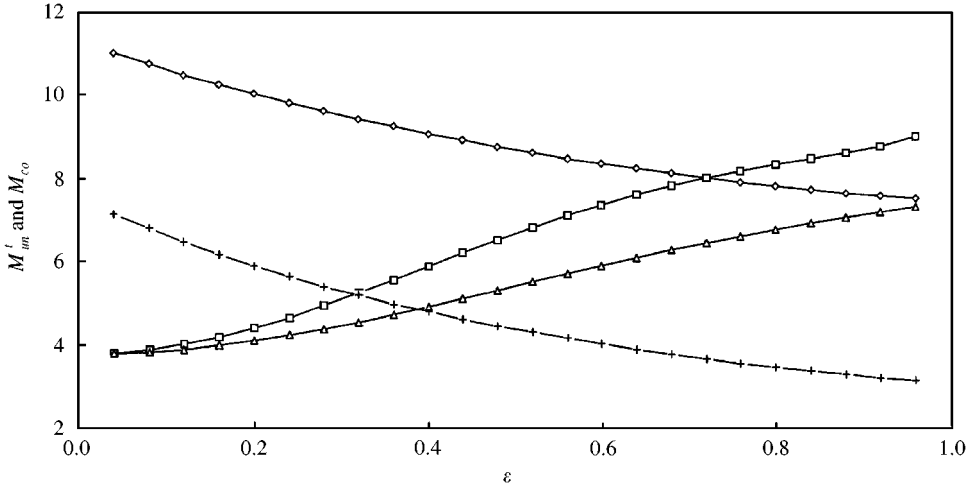


Figure 5. Tangential inertia force coefficient comparison for long model: —◇—, M_{un}^t (present); —□—, M_{co} (El-Shafei & Crandall); —+—, M_{co} (present); —△—, M_{un}^t , (El-Shafei & Crandall).

TABLE 7

Force coefficients for the long cylindrical model from using the present energy method and El-Shafei's parabolic velocity profile

C_v^n	$\frac{12\pi}{\gamma^3}$	C_v^t	$\frac{24\pi}{(2 + \varepsilon^2)\gamma}$
M_{un}^n	$\frac{24\pi}{10\varepsilon^2}(1 - \gamma)$	M_{un}^t	$\frac{2.4\pi}{\varepsilon^2(2 + \varepsilon^2)}[2\varepsilon + \varepsilon^3 + 2\gamma(1 - \varepsilon) - 2\gamma^2]$
M_{cv}	$-\frac{24\pi}{10\varepsilon^2}\left(1 - \frac{2 - \varepsilon^2}{2\gamma}\right)$	M_{co}	$\frac{6\pi}{35\varepsilon\gamma(2 + \varepsilon^2)}(4 - 4\gamma - 10\varepsilon + 7\varepsilon^2 + 24\varepsilon\gamma - \varepsilon^3 - 2\varepsilon^2\gamma)$
M_{ce}	$\frac{12\pi}{35(2 + \varepsilon^2)^2}(-6 - 3\varepsilon^2 + 20\gamma + \gamma\varepsilon^2)$		

direction. The two tangential inertia coefficients, M_{un}^t and M_{co} , in Figure 5 show remarkably different trends compared to El-Shafei & Crandall (1991). For very small eccentricities ($\varepsilon \rightarrow 0$), all the tangential force coefficients obtained here are 2 or 3 times bigger. When $\varepsilon \rightarrow 1$, there are still clear differences in the Coriolis inertia force coefficient M_{co} from the two methods, whereas C_v^t and M_{un}^t approach similar values.

To help to understand the squeeze film force differences caused by the difference between the two parabolic velocity profiles in the third term of $v_c'(3\varepsilon/(2 + \varepsilon^2))$, a derivation was also carried out using the present energy approximation method and the parabolic velocity distribution obtained by El-Shafei (1988). The results are shown in Table 7. Except for M_{ce} , M_{un}^t and M_{co} , all the other force coefficients are exactly the same as obtained by El-Shafei & Crandall (1991) and shown in Table 6. Figure 6 shows these three inertia force coefficients versus instantaneous eccentricity, derived using the two velocity distributions. It demonstrates that the differences are quite big (two or three times) for small eccentricities. As the eccentricity increases, the differences become smaller. At large eccentricities ($\varepsilon \rightarrow 1$) the differences are very small. All three dashed curves in Figure 6 (using the present energy

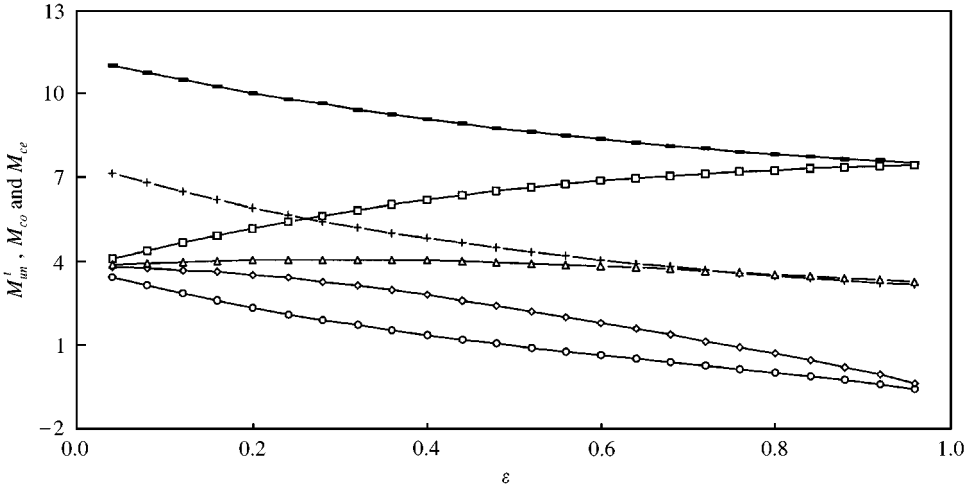


Figure 6. Three long model inertia force coefficients from the present energy method with El-Shafei’s velocity profile and with the present parabolic velocity profile; —■—, M'_{um} (present); —□—, M'_{um} (El-Shafei & Crandall); —+—, M'_{co} (present); —△—, M'_{co} (El-Shafei & Crandall); (—◇—, M'_{ce} (El-Shafei & Crandall); —○—, M'_{ce} (present).

method with El-Shafei’s velocity profile) have values near 4 at low eccentricities, which is what El-Shafei & Crandall (1991) predict (see Figures 4 and 5).

For further comparison, the expressions for a long squeeze film damper performing circular orbits about the centre of the bearing housing from San Andres & Vance (1986) for $Re \ll 1$ and $Re \rightarrow \infty$ are examined. The only nonzero inertia coefficient is the centripetal term M_{ce} and C_v is the only viscous term. Their M_{ce} coefficient can be expressed as

$$M_{ce} = \begin{cases} \frac{12\pi}{35} \left[\frac{\gamma - 1}{\varepsilon^2} \left(1 + \frac{2\gamma}{2 + \varepsilon^2} \right) + \frac{18\gamma}{(2 + \varepsilon^2)^2} \right] & Re \ll 1, \\ \frac{4\pi\gamma}{(2 + \varepsilon^2)^2} & Re \rightarrow \infty. \end{cases} \tag{29}$$

Their expression for C'_v is the same as El-Shafei & Crandall’s in Table 6. The variations of M_{ce} with ε along with results from El-Shafei & Crandall (1991) and the present study, are shown in Figure 7. The above two expressions of M_{ce} for small and large Reynolds numbers have very similar trends as ε changes. The results of the present energy method with two different parabolic velocity profiles [one of them contains the term with $3\varepsilon/(2 + \varepsilon^2)$] are also shown in Figure 7. From Table 7, Figure 7 and the above expressions, we see that the inertia force coefficients M_{ce} from the present energy method (with both parabolic velocity profiles) and from the study by San Andres & Vance have no big differences for different instantaneous eccentricity ratios.

From the above comparisons, the following six observations can be made for the long model. (i) The only differences among the present squeeze film force equations due to the three approximation methods and the two different velocity profiles are in the four constant D_i coefficients and the differences are generally not very big. (ii) Three of the four normal-direction force coefficients (all but M_{ce}) are exactly the same as El-Shafei & Crandall (1991) (when the same D_i factors are used). (iii) The variation of M_{ce} with ε is very similar to that found by San Andres & Vance (1986), although it is very different from El-Shafei & Crandall (1991), especially for $\varepsilon \gg 0$. (iv) The tangential-direction viscous force coefficient is approximately

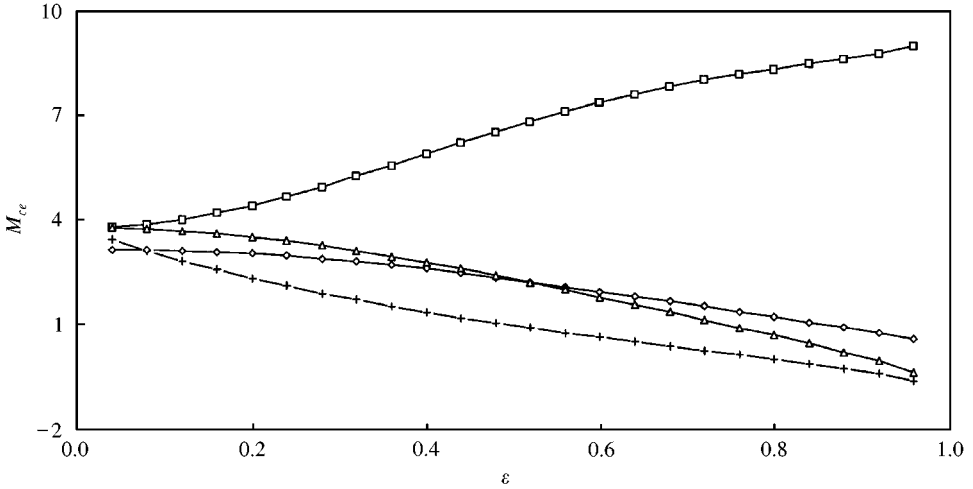


Figure 7. Centripetal inertia force coefficient (M_{ce}) for circular-centered motions for long model: —□—, El-Shafei & Crandall; —◇—, San Andres & Vance for $Re \rightarrow \infty$; —△—, San Andres & Vance for $Re \rightarrow 0$ and present method with El-Shafei's velocity profile; —+—, present method with present parabolic velocity profile.

3 times larger than El-Shafei & Crandall's as $\varepsilon \rightarrow 0$, but becomes comparable for $\varepsilon \gg 0$. (v) The two tangential-direction inertia force coefficients M_{un}^t and M_{co} in the present model show very different trends with ε compared to El-Shafei & Crandall; although they are roughly comparable in size, in the present model they decrease as ε increases, whereas El-Shafei & Crandall predicted the opposite trend. (vi) When the present energy method and the parabolic velocity profile with $3\varepsilon/(2 + \varepsilon^2)$ is used, the inertia force coefficients M_{un}^t and M_{co} show big differences from El-Shafei & Crandall (1991) as $\varepsilon \rightarrow 0$, but become similar for $\varepsilon \gg 0$.

The above discussion indicates that the normal force components in the long model show quite good agreement with previous models. [The centripetal term by El-Shafei & Crandall (1991) appears to be inconsistent with both the present work and that of San Andres & Vance (1986).] In contrast the present results for the tangential force terms are substantially different from previous models.

The studies by El-Shafei & Crandall and those of San Andres & Vance are based on the assumptions of small amplitude arbitrary or circular-centred motions, respectively. The present effort aimed to include the large fluid inertia effects due to large amplitude cylinder (journal) motions. The significant differences in the final force equations are due to the different assumptions used in the derivation of the force equations. The present force equations with the elliptical velocity profile should lead to more accurate results for high squeeze Reynolds numbers, since when $Re > 50$ the parabolic velocity profile from El-Shafei & Crandall (1991) has large differences from the real velocity profiles as demonstrated by Han & Rogers (1996). To verify the accuracy of the present analytical models, experimental tests and more theoretical work are needed.

4. CONCLUSIONS

Using three approximation methods and two velocity profiles, both short and long cylindrical squeeze film force models have been developed. The nonlinear force equations have the same form for the two models.

Comparisons with the existing models demonstrates that the force terms in the present short cylindrical squeeze films are either exactly the same or have the same trends with instantaneous eccentricity values. The differences resulting from different averaging methods and velocity profiles are not very large.

Comparing the present expressions obtained using the present parabolic velocity profile with existing models for long cylindrical squeeze films illustrates that: (i) the viscous, unsteady inertia and convective inertia terms, acting in the normal direction, are essentially the same as in other studies; (ii) the normal direction centripetal inertia term shows similar variations with position as one published study, but very different from another study; and (iii) the three tangential direction force terms show variations with position which are very different from a previous published study.

The higher unsteady inertia forces obtained using the iterative and energy approximation methods, along with the elliptical velocity profiles, show that the new models include larger inertia effects. The unsteady inertia force coefficients obtained using the elliptical velocity profile is about 1.1–1.2 times higher than those obtained using El-Shafei & Crandall's parabolic velocity profile when either the iterative or energy approximation method is used. The present models should predict more accurately the squeeze film forces acting between tubes and their support plates in shell-and-tube heat exchangers.

ACKNOWLEDGEMENT

The work reported here was supported by Atomic Energy of Canada Limited as part of its work on heat exchanger tube vibration and wear prediction. The authors also acknowledge the support of the Natural Sciences and Engineering Research Council of Canada and the University of New Brunswick.

REFERENCES

- BARRETT, L. E., ALLAIRE, P. E. and GUNTER, E. J. 1980 A finite length bearing correction factor for short bearing theory. *ASME Journal of Lubrication Technology* **102**, 283–287.
- BOOKER, J. F. 1965 A table of the journal-bearing integral. *ASME Journal of Basic Engineering* **87**, 533–535.
- EL-SHAFAEI, A. 1988 Dynamics of rotors incorporating squeeze film dampers. Ph.D. Dissertation, Department of Mechanical Engineering, Massachusetts Institute of Technology, Cambridge MA, U.S.A.
- EL-SHAFAEI, A. & CRANDALL, S. H. 1991 Fluid inertia forces in squeeze film dampers. In *Rotating Machinery and Vehicle Dynamics* **35**, pp. 219–228. New York: ASME.
- ESMONDE, H., FITZPATRICK, J. A., RICE, H. J. & AXISA, F. 1992 Modelling and identification of nonlinear squeeze films dynamics. *Journal of Fluids and Structures* **6**, 223–248.
- HAN, Y. 1997 Nonlinear fluid forces in cylindrical squeeze films. Ph.D. Dissertation, Department of Mechanical Engineering, University of New Brunswick, Fredericton, Canada.
- HAN, Y. & ROGERS, R. J. 1996 Squeeze film force modelling for large amplitude motion using an elliptical velocity profile. *ASME Journal of Tribology* **118**, 687–692.
- HAN, Y. & ROGERS, R. J. 1997 Nonlinear models for long cylindrical squeeze films incorporating elliptical velocity profiles. Proceedings of the Fourth International Symposium on Fluid-Structure Interactions, Aeroelasticity, Flow-Induced Vibration & Noise **AD-53-2**, **41** pp. 473–482. New York: ASME.
- HAN, Y. & ROGERS, R. J. 2001 Nonlinear fluid forces in cylindrical squeeze films. Part II: Finite length. *Journal of Fluids and Structures* **15**, 171–206, doi:10.1006/jfls.2000.0325.
- HASLINGER, K. H., MARTIN, M. L. & STEININGER, D. A. 1990 Experimental characterization of fluid and squeeze film effects in heat exchanger tube supports. *Journal of Fluids and Structures* **4**, 605–629.
- JUNG, S. Y. 1990 Effects of fluid inertia and cavitation on the force coefficients of a squeeze film damper. PhD Dissertation, Department of Mechanical Engineering, Texas A&M University, College Station, TX, U.S.A.

- LU, Y. 1993 Instantaneous squeeze film force between a heat exchanger tube and a support plate. Ph. D. Dissertation, Department of Mechanical Engineering, University of New Brunswick, Fredericton, Canada.
- LU, Y. & ROGERS, R. J. 1992 A nonlinear model for short length, cylindrical squeeze films with large planar motions. *ASME Journal of Tribology* **114**, 192–198.
- LU, Y. & ROGERS, R. J. 1994 Normal instantaneous squeeze film force for a finite length cylinder. *ASME Journal of Tribology* **116**, 588–596.
- LU, Y. & ROGERS, R. J. 1995 Instantaneous squeeze-film force between a heat exchanger tube and a support plate for arbitrary tube motion. *Journal of Fluids and Structures* **9**, 835–860.
- MULCAHY, T. M. 1980 Fluid forces on rods vibrating in finite length annular regions. *Journal of Applied Mechanics* **47**, 234–240.
- PETTIGREW, M. J. & KO, P. L. 1980 A comprehensive approach to avoid vibration and fretting in shell-and-tube heat exchangers. In *Flow-Induced Vibration of Power Plant Components*, Vol. **PVP-41**, pp. 1–18. New York: ASME.
- PETTIGREW, M. J., ROGERS, R. J. & AXISA, F. 1986 Damping of multispans heat exchanger tubes — Part 2: In liquids. In *Flow Induced Vibration — 1986*, PVP-104, pp. 89–98. New York: ASME.
- SAN ANDRES, L. A., MENG, G. & YOON, S. 1993 Dynamic force response of an open-ended squeeze film damper. *ASME Journal of Engineering for Gas Turbines and Power* **115**, 341–346.
- SAN ANDRES, L. A. & VANCE, J. M. 1986 Effects of fluid inertia and turbulence on the force coefficients for squeeze film dampers. *ASME Journal of Engineering for Gas Turbines and Power* **108**, 332–339.
- SAN ANDRES, L. A. & VANCE, J. M. 1987a Effects of fluid inertia on squeeze-film damper forces for small-amplitude circular-centered motions. *ASLE Transactions* **30**, 63–68.
- SAN ANDRES, L. A. & VANCE, J. M. 1987b Force coefficients for open-ended squeeze-film dampers executing small-amplitude motions about an off-center equilibrium position. *ASLE Transactions* **30**, 69–76.
- TICHY, J. A. 1982 Effects of fluid inertia and viscoelasticity on squeeze-film bearing forces. *ASLE Transactions* **25**, 125–132.
- TICHY, J. A. 1984 Effects of fluid inertia and viscoelasticity on the one-dimensional squeeze-film bearing. *ASLE Transactions* **27**, 164–167.
- TICHY, J. A. 1985 Measurement of squeeze-film bearing forces and pressures, including the effect of fluid inertia. *ASLE Transactions* **28**, 520–526.
- TICHY, J. A. & BOU-SAID, B. 1991 Hydrodynamic lubrication and bearing behaviour with impulsive loads. *STLE Tribology Transactions* **34**, 505–512.
- WARNER, P. C. 1963 Static and dynamic properties of partial journal bearings. *ASME Journal of Basic Engineering* **85**, 247–257.
- ZHANG, J. X. 1997 Fluid inertia effects on the performance of short and long squeeze film dampers executing periodic vibration. *ASME Journal of Tribology* **119**, 306–314.
- ZHANG, J., ELLIS, J. & ROBERTS, J. B. 1993 Observations on the nonlinear fluid forces in short cylindrical squeeze film dampers. *ASME Journal of Tribology* **115**, 692–698.
- ZHANG, J. & ROBERTS, J. B. 1996 Solutions for the combined motion of finite length squeeze film dampers around the bearing center. *ASME Journal of Tribology* **118**, 617–622.
- ZHANG, J., ROBERTS, J. B. & ELLIS, J. 1994 Experimental behavior of a short cylindrical squeeze film damper executing circular centered orbits. *ASME Journal of Tribology* **116**, 528–534.

APPENDIX A: DERIVATION OF PRESSURE GRADIENTS FOR LONG MODELS

A.1. MOMENTUM METHOD

Considering that the three terms on the left-hand side of equation (7) are functions of y and the fact that the squeeze film is very thin ($h \ll R$), an averaging procedure can be taken for the three terms to solve the equation. Then, the equation is changed into

$$\frac{\rho}{h} \int_0^h \left(\frac{\partial u}{\partial t} + u \frac{\partial u}{R \partial \theta} + v \frac{\partial u}{\partial y} \right) dy = - \frac{\partial p}{R \partial \theta} + \mu \frac{\partial^2 u}{\partial y^2}. \quad (\text{A1})$$

Using equations (22) and (23) and taking into account that $v_c = \partial h / \partial t$ and $\partial h / \partial \theta = e \sin \theta$, we can then obtain $\partial p / \partial \theta$ with the parabolic velocity profile

$$\frac{\partial p}{\partial \theta} = -\frac{12\mu R^2}{h^3} v'_c - \frac{\rho R^2}{h} C_t^1 - \frac{12\rho R^2}{5h^2} C_t^2 + \frac{6\rho R^2}{5h^3} C_\theta^2. \quad (\text{A2})$$

Similarly, using equations (18) and (21), $\partial p / \partial \theta$ with the elliptical velocity profile is

$$\begin{aligned} \frac{\partial p}{\partial \theta} = & -\frac{8\mu R^2}{Bh^3} \frac{v'_c}{E_2} - \frac{\rho R^2}{h} C_t^1 - \frac{8\rho R^2}{B^2 h^2} \left[A^2(1 - E_2 E_4) - \frac{1}{3} \right] C_t^2 \\ & + \frac{4\rho R^2}{B^2 h^3} \left[A^2(1 - E_2 E_4) - \frac{1}{3} \right] C_\theta^2. \end{aligned} \quad (\text{A3})$$

In the above equations,

$$C_t^1 = \ddot{e} \sin \theta + \dot{e} \dot{\psi} (1 - 2 \cos \theta) + e \ddot{\psi} (1 - \cos \theta) - e \dot{\psi}^2 \sin \theta,$$

$$C_t^2 = -v_c v'_c, \quad C_\theta^2 = v_c'^2 e \sin \theta,$$

and v_c and v'_c are defined in equations (11) and (15), respectively.

A.2. ITERATIVE METHOD

Rearranging the simplified Navier–Stokes equation (7) for the infinitely long cylindrical squeeze film shown in Figure 1 for $\partial^2 u / \partial y^2$, we have

$$\frac{\partial^2 u}{\partial y^2} = \frac{1}{\mu} \left[\frac{\partial p}{R \partial \theta} + \rho \left(\frac{\partial u}{\partial t} + u \frac{\partial u}{R \partial \theta} + v \frac{\partial u}{\partial y} \right) \right]. \quad (\text{A4})$$

Since p is a function of θ and t , after substituting equations (18) and (21) and equations (22) and (23), respectively, into the above equation, solutions for u can be obtained by integrating the above equation twice with respect to y . To make the integration, the geometric condition

$$y = h/2, \quad \partial u / \partial y = 0 \quad (\text{A5})$$

and the boundary condition

$$u = 0, \quad y = 0 \quad (\text{A6})$$

are used.

The derived velocity distribution has to satisfy the continuity relationship for the cylindrical squeeze film configuration

$$\int_0^h u \, dy = - \int_0^\theta \frac{dh}{dt} R \, d\theta = R v'_c. \quad (\text{A7})$$

Substituting for the expressions for u into the above equation and making the integral directly, we obtain $\partial p / \partial \theta$ for the parabolic velocity profile

$$\frac{\partial p}{\partial \theta} = -\frac{12\mu R^2}{h^3} v'_c - \frac{6\rho R^2}{5h} C_t^1 - \frac{102\rho R^2}{35h^2} C_t^2 + \frac{54\rho R^2}{35h^3} C_\theta^2, \quad (\text{A8})$$

and for the elliptical velocity profile

$$\begin{aligned}
\frac{\partial p}{\partial \theta} = & -\frac{12\mu R^2}{h^3} v'_c - \frac{\rho R^2}{8hB} [(3A^2 - 10)E_2 + 3(4 - A^2)A^2E_4]C_t^1 \\
& - \frac{\rho R^2}{4h^2B} [-(3A^2 + 14)E_2 + 3(A^2 - 4)A^2E_4 + 24A]C_t^2 \\
& - \frac{\rho R^2}{h^2B^2} \left[\frac{1}{10} + \frac{A^2}{12}(119 - 69A^2) + A^2E_2E_4 \left(\frac{23}{4}A^2 - 11 \right) \right] C_t^3 \quad (A9) \\
& - \frac{\rho R^2}{h^2B^2} [3A(A^3E_4^2 - 2A^2E_4 + 2E_2)]C_t^2 \\
& + \frac{\rho R^2}{10h^3B^2} [65A^2 - 18 - 15A^2E_2E_4(4 - A^2) - 15A^4]C_\theta^2.
\end{aligned}$$

A.3. ENERGY METHOD

According to El-Shafei (1988), using an energy method, the Navier–Stokes equation is multiplied by the circumferential flow velocity prior to integration across the film to obtain the average circumferential pressure gradient. The equation for the energy method is

$$\frac{\partial p}{R \partial \theta} = -\rho \frac{\int_0^h u(\partial u/\partial t) dy}{\int_0^h u dy} + \mu \frac{\int_0^h u(\partial^2 u/\partial y^2) dy}{\int_0^h u dy} - \rho \frac{\int_0^h u(u(\partial u/R \partial \theta) + v(\partial u/\partial y)) dy}{\int_0^h u dy}. \quad (A10)$$

Substituting equations (18) and (21) and equations (22) and (23), respectively, we again find equation (A8) for the parabolic velocity profile, and for the elliptical velocity profile

$$\begin{aligned}
\frac{\partial p}{\partial \theta} = & -\frac{16\mu R^2}{B^2h^3} \left[\frac{A}{2} \ln \left(\frac{A+1}{A-1} \right) - 1 \right] v'_c - \frac{4\rho R^2}{B^2h} \left[A^2(1 - E_2E_4) - \frac{1}{3} \right] C_t^1 \\
& - \frac{\rho R^2}{B^2h^2} \left[2 \left(A^2(1 - E_2E_4) - \frac{1}{3} \right) + \frac{3}{2B} (E_2(2 - 15A^2)) \right. \\
& \left. + A^2E_4(15A^2 - 12) \right] C_t^2 \\
& + \frac{\rho R^2}{B^3h^3} [E_2(2 - 15A^2) + A^2E_4(15A^2 - 12)]C_\theta^2. \quad (A11)
\end{aligned}$$

A.4. GENERAL PRESSURE GRADIENT AND SQUEEZE FILM FORCES

We can write the pressure gradient for each method as

$$\frac{\partial p}{\partial \theta} = -\frac{\mu R^2}{h^3} D_1 v'_c - \frac{\rho R^2}{h} D_2 C_t^1 - \frac{\rho R^2}{h^2} D_3 C_t^2 + \frac{\rho R^2}{h^3} D_4 C_\theta^2. \quad (A12)$$

The effects of using a different approximation method or the elliptical or parabolic profiles are entirely contained in the expressions for the constant coefficients, D_i ($i = 1-4$). Values for the D_i coefficients are shown in Tables 1 and 2.

Squeeze film force equations (25) and (26) can be conveniently integrated using the method of integration by parts. Treating the pressure far from the film edge as zero

we have

$$F_n = -C_1 D_1 \sum_{j=1}^2 F_{1j}^n - C_2 D_2 \sum_{j=1}^4 F_{2j}^n - C_3 D_3 \sum_{j=1}^3 F_{3j}^n + C_3 D_4 \sum_{j=1}^3 F_{4j}^n, \quad (\text{A13})$$

$$F_t = C_1 D_1 \sum_{j=1}^2 F_{1j}^t + C_2 D_2 \sum_{j=1}^4 F_{2j}^t + C_3 D_3 \sum_{j=1}^3 F_{3j}^t - C_3 D_4 \sum_{j=1}^3 F_{4j}^t. \quad (\text{A14})$$

The geometric coefficients C_i in the above equations are listed in Table 5. The force components in the normal and tangential directions in the equations can be found in Han (1997). For the limit of $(0, 2\pi)$, through rearranging equations (A13) and (A14), we have equations (27) and (28).

APPENDIX B: NOMENCLATURE

A	shape factor of elliptical velocity profile (ratio of ellipse minor axis to h)
c	radial clearance
C_i	geometry coefficients, $i = 1, 2, 3$
C_v	viscous (damping) force coefficient
D, R	cylinder diameter and radius
D_i	constant force coefficients, $i = 1, 2, 3, 4$
e	amplitude of the cylinder sinusoidal motion
F	squeeze film force on the cylinder
h	instantaneous local squeeze film thickness
L	cylinder length
M_{ce}	centripetal inertia force coefficient
M_{co}	Coriolis inertia force coefficient
M_{cv}	convective inertia force coefficient
M_{un}	unsteady inertia force coefficient
p	pressure in squeeze film
p_a	pressure far from the film edge
p_c	mid-plane pressure
Re	squeeze film Reynolds number ($\text{Re} = \omega c^2/\nu$)
u, v	flow velocities in circumferential and radial directions
x, y, z	moving coordinate directions (Figures 1 and 2)
X, Y, Z	fixed coordinate directions (Figures 1 and 2)
γ	$(1 - \varepsilon^2)^{1/2}$
ε	instantaneous eccentricity ratio e/c
θ, φ	angles (Figures 1 and 2)
μ	absolute fluid viscosity
ν	kinematic fluid viscosity
ρ	fluid mass density
$\psi, \dot{\psi}, \ddot{\psi}$	instantaneous angle, angular velocity and acceleration of cylinder centre
ω	characteristic circular frequency